CARBON letters

Note

Carbon Letters Vol. 26, 95-101 (2018)

The effect of carbon nanotube diameter on the electrical, thermal, and mechanical properties of polymer composites

Kyung Jae Kim[1,2], Mong-Young Huh[1], Won-Seok Kim[1], Joon-Hyuk Song[1], Hak Sung Lee[1], Ji-Yeon Kim[3], So-Ra Lee[2], Won Seok Seo[4], Sung-Mo Yang[5], and Young Soo Park[1,♠]

[1]Korea Institute of Carbon Convergence Technology, Jeonju 54853, Korea
[2]Department of Machine Design Engineering, Chonbuk National University, Jeonju 54896, Korea
[3]Department of Information & Communication Engineering, Wonkwang University, Iksan 54538, Korea
[4]Department of Chemistry, Seogang University, Seoul 04107, Korea
[5]Departmemnt of Machine System Engineering, Chonbuk National University, Jeonju 54896, Korea

Article Info
Received 5 July 2017
Accepted 10 October 2017

♠Corresponding Author
E-mail: ironny@kctech.re.kr
Tel: +82-63-219-3721

Open Access
DOI: http://dx.doi.org/10.5714/CL.2018.26.095

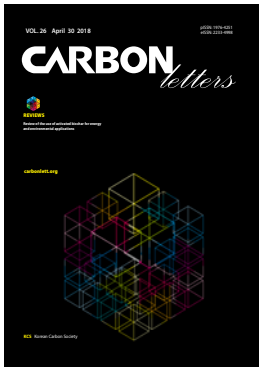

http://carbonlett.org

pISSN: 1976-4251
eISSN: 2233-4998

It is well-known that carbon nanotubes (CNTs) have unique properties: thermal conductivity of 3000 W/m·K, electrical resistivity of (5 to 50) μΩ·cm, and tensile strength of about 50 GPa [1-4]. These promising properties have attracted the interest of researchers studying CNT-polymer composites in a variety of fields including electromagnetic wave shielding, heat spreaders, and high strength structures [5-9]. Despite this effort, there has been limited improvement in the thermal conductivity and mechanical properties of composite materials. One of the most fundamental problems in improving the properties of CNT-based composites has been controlling the CNT diameter and length. Change in the diameter of carbon nanotubes directly affects CNT characteristics, and CNTs with larger diameters are known to have increased defect density and diminished CNT characteristics [10]. Kis and Zettl [11] found that the Young's modulus of CNT decreases with decreasing particle diameter. Fujii *et al*. [4] experimentally demonstrated that the thermal conductivity of CNTs decreased rapidly from (3000 to 500) W/m·K when the diameter increased from (8 to 30) nm.

It was proposed that the diameter of as-grown carbon nanotubes was defined by the size of the catalysts used in chemical vapor deposition (CVD). Cheung *et al*. [12] achieved diameter-controlled synthesis of carbon nanotubes using size-adjusted Fe catalyst on a silicon substrate. Moreover, Ding *et al*. [13] reported that CNT diameters were similar to the sizes of the Fe particles after synthesis simulation using iron clusters of various sizes. Based on these, many researchers have tried to synthesize CNTs of various diameters to research the properties of CNT-reinforced composites according to their diameters. As a result, single-walled carbon nanotubes (SWNTs), which are known to be excellent, high-quality multifunctional fillers, have limited applicability due to their low purity and high cost. Commercial CNTs with diameters in the range 10–30 nm solved the cost problem, but their applications for reinforced composites were limited due to their low crystallinity. Thin CNTs with small diameters (e.g., < 10 nm) and higher crystallinity than commercial CNTs, were proposed as alternatives to solve this problem [14-16], but thin CNTs have not yet been commercialized for use in composites.

For this paper, we investigated the effect of fine catalyst composition on carbon nanotube structure, diameter, crystallinity and yield for low diameter CNT synthesis. Then, once the polyamide composites had been characterized according to the CNT diameters and contents, these were used to select CNTs with more suitable diameters for composites.

The materials used for catalyst were as follows. Ammonium molybdate tetrahydrate (98.5 % assay), iron(III) nitrate nonahydrate, citric acid anhydride, and magnesium nitrate hexahydrate were purchased from Daejung Chemicals & Metals Co., Ltd. (Korea). All reagents were of extra pure grade and were used without further purification. The gases used for synthesis of CNTs were methane, hydrogen, and argon gas. All gases (99.5 % purity) were purchased from Hankook Special Gas Co., Ltd. (Korea). The polyamide used for the polymer matrix, named elvamide 8063, is soluble in ethanol and was purchased from Du-

pont, Ltd. (USA). Ethanol with 98.5 % purity for dissolving the polyamide was purchased from Daejung Chemicals & Metals Co., Ltd. (Korea).

To control the CNT diameter, catalysts were synthesized at 600°C using a combustion method [17]. The procedure for catalyst preparation was as follows. All catalysts were prepared based on 100 g of magnesium nitrate and 35 g of citric acid. Portions of ammonium molybdate and iron nitrate were weighed so that the molar amount of Mo would be in the range (0.01 to 0.10) mol and the molar amount of Fe would be in the range (0.01 to 0.02) mol. Then, ammonium nitrate, magnesium nitrate, and citric acid (in this order) were added to 100 g of boiling water. Iron nitrate was dissolved in 30 mL of ethanol and added last. The aqueous solution in which the four salts were dissolved was boiled and vigorously mixed for about 20 min using a magnetic stirrer. Then, the solution was put in a furnace pre-heated to 600 °C for 15 min to prepare catalyst powder. To prevent oxidation of the catalysts, the stainless steel vessel was capped during the combustion process. About 20 % of the carbonated citric acid (compared to the total catalyst calculated) remained due to vessel capping. This resulted in a brown catalyst rather than yellow or slightly red catalyst. The catalyst powder was pulverized for 20 s using a household blender to obtain a fine catalyst powder. A Thermal-CVD reactor (Atech System, Ltd., Korea) was used for CNT synthesis. The CVD reactor was heated to 920 °C (synthesis temperature) under argon gas. After a catalyst was put into the reactor, a mixture of hydrogen (at 1 SLM) and methane (at 3 SLM) were supplied instead of argon, and were kept flowing for 40 min to synthesize CNTs. After the reactor cooled down to 300°C, the as-grown CNT powders were collected. The yield of synthesized CNT was calculated by the CNT content relative to the catalyst input, and calculated according to the following formula.

Yield_CNT = (amount of CNT gained – amount of catalyst) / amount of catalyst

To investigate the diameter distribution of the as-grown CNTs, they were dispersed in ethanol and dropped onto a carbon-coated nickel TEM grid. CNTs were observed using a TEM (Jeol JEM-2100, Jeol, Japan). The average diameter and diameter distribution of the CNTs were obtained by measuring the diameters of approximately 100 CNTs from TEM images. The CNT morphology was analyzed using FE-SEM (Hitachi S-4800, Hitachi Hi Tech. Co., Japan) without any treatment. The length of the CNTs was analyzed using SEM after filtering ultrasonic-dispersed CNTs with 200 nm pore-size polycarbonate membrane. The crystallization of pristine CNTs was measured using Raman (532 nm, Horiba LabRam-HR, Horiba, Ltd., Japan). The degree of crystallization was the peak area ratio from D-peak (around 1350 cm^{-1}) to G-peak (1580 cm^{-1}) in the Raman spectra. For calculation of peak area, curve fitting was carried out using the Lorentz distribution method. To determine the interlayer spacing and crystallinity of CNTs, a wide angle X-ray diffraction device (XRD, X'pert-PROMPD powder Diffractometer, PANalytical, Netherlands) equipped with a rotation anode using CuKα radiation (λ = 0.1532 nm) was used. All CNTs were purified before measuring. For the pore analysis, the amount of N_2 gas adsorbed was measured at 77 K with relative pressure (P/P_0) using BELSORP (Microtrac BEL Co., Ltd., Japan). The specific surface area was calculated from the isothermal adsorption curve using the BET equation. Prior to measurement, all CNTs were outgassed at 300°C for 2 h to obtain a residual pressure of less than 10^{-2} Torr.

CNT-Polyamide composites were produced through solution blending while changing the CNT content from 1 phr (parts per hundred rubber) to 50 phr. The polyamide-ethanol solution was prepared by slowly adding polyamide to ethanol to reach 10 wt% and stirring vigorously for 4 h at 60°C. To minimize the influence of the remaining catalyst and acid on the composites, 3 mol nitric acid aqueous solution was used to remove the used catalyst. The dissolved metal ions and acid were removed by several washings with deionized water. The purified CNTs were ground in water for two hours using a 6000 RPM homogenizer. Crushed CNTs were only filtered, and then were used for mixing without drying to prevent agglomeration. The dispersion of CNTs in the polyamide was accomplished using 60 % output of 700 W bar-type ultrasound for 60 min. The mixed solution of CNTs and polyamide was put into cold water and solidified. Then the mixture of CNT-polyamide was dried at 100 °C for 12 h. The dried CNT-polyamide composites were compressed to 400 kgf using a hot press in the range 150–180 °C to produce 1 mm-thick CNT-polyamide composites. To observe the dispersion state of CNTs in the composite material with an optical microscope (BX51, Olympus Co.), specimens were prepared by pressing a few drops of polyamide-ethanol solution containing dispersed CNT on a polyimide film.

Measurement of the electric resistivity of nano-composite sheets ~ 1mm thick and 150 mm in diameter was carried out at room temperature using a conventional four point probe technique (Loresta-GP M610, Mitsubishi Chemical Co., Japan). Rectangular samples 22 mm thick and of different thicknesses were prepared for thermal conductivity. To determine the thermal conductivity of composites, the same samples of different thicknesses were measured twice using a thermal conductivity meter (ThermoCon M100, Metrotech Co., Ltd., Korea) in accordance with the ASTM D 5470 standard. In this method, thermal conductivity is defined as the ratio of heat flux to the associated thermal gradient under one-dimensional heat conduction conditions. This measurement could be envisioned as thermal conduction between two parallel, isothermal surfaces of area A, at temperatures T_H and T_L, separated by a layer of composites having a thickness with a steady state power of Q. Thermal conductivity, k, was thus defined as

$$k = Q \times X / ((T_H - T_L) \times A)$$

Tensile specimens were prepared by cutting the composites with a specimen cutter knife to the type V dimensions in accordance with ASTM D 638-03. The tensile properties of the composites were measure using an Instron-3382 (Instron, USA) at a cross-head speed of 5.0 mm/min. All measurement was conducted at room temperature and the average value reported was obtained from three independent samples.

Diameter control of the CNTs was achieved by adjusting the ratio of the amount of Fe-Mo used to the amount of magnesium oxide used as a support. In order to determine the proper Fe content in the catalysts, the amount of Fe was varied in the range 0.01–0.05 mol. Through SEM observation, it was confirmed that

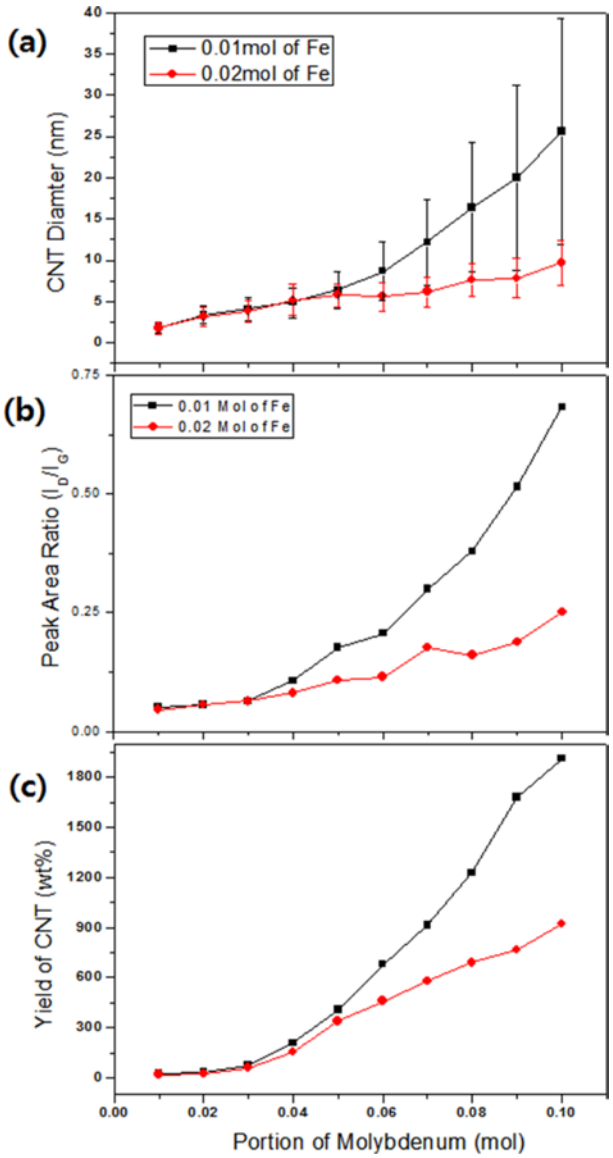

Fig. 1. The characteristic of as-grown CNTs according to the portion of Mo in Mo-Fe/MgO catalysts. (a) Diameter distributions, (b) Raman spectra, and (c) Yields.

CNTs or carbon nano fibers (CNFs) having a diameter of 30 nm or more, were present in CNT samples with 0.03 mol or more of Fe. The optimal amount of Fe was determined to be in the range 0.01–0.02 mol. CNTs were synthesized by changing the Mo content from (0.01 to 0.10) mol while the Fe content was fixed at (0.01 and 0.02) mol, respectively.

Fig. 1 shows the diameter distribution, crystallinity, and yield of CNTs synthesized with increasing molybdenum content at the two different iron contents. From Fig. 1(a), the rate of change of the CNT diameter slightly increases with low Mo content, but the rate of change of diameter according to iron content differs significantly at high Mo content. In the case of 0.02 mol of iron, the increases in the diameter and diameter distributions were not relatively wide. In the case of 0.01 mol of iron, the diameter distribution of the CNTs was very broad and the average diameter was also dramatically increased. Looking more closely at the graph, it can be seen that the mean diameter and diameter distribution are similar when the amount of Mo is below 0.04 mol. However, at 0.05 mol of Mo, the average diameter is similar but the diameter distribution is different. Moreover, the average diameter is 6 nm and 12 nm for 0.07 mol of molybdenum. When the molybdenum content was increased to 0.10 mol, the average diameter and the diameter distribution were found to be 25 nm and 10–35 nm, respectively, in 0.01 mol of iron content. On the other hand, in the case of 0.02 mol of iron, the average CNT diameter was as small as 10 nm and the diameter distribution was as narrow as 7–13 nm. Raman spectra of the kinds of CNT are shown in Fig. 1(b). The crystallinity of CNT is generally defined by the ratio of the integrated D-peak intensity (A_D) to the integrated G-peak intensity (A_G; i.e., A_D/A_G) in the Raman spectrum of CNT. From the graph, it can be seen that, as the content of Mo increased, the crystallinity of both iron catalysts decreased. Moreover, the rate of decline of the crystallinity at high iron content occurred with Mo content of 0.03 mol or less. The A_D/A_G value was less than 0.06 at all Fe contents. This indicates that the CNT had very high crystallinity. The crystallinity difference between CNTs of the two iron catalysts began to be observed at 0.04 mol, and the crystallinity difference became larger as the Mo content increased. That is, in the case of 0.07 mol of Mo, the degree of A_D/A_G was 0.24 and 0.16, respectively. The crystallinity further decreased at 0.10 mol of Mo, and the A_D and A_G values were 0.30 and 0.18, respectively. This tendency was similar to those of the mean diameter and diameter distribution with variation of the Mo content, as mentioned above.

Fig. 1(c) shows the yields of CNT according to the Mo content. Yield was calculated as the ratio of the amount of CNT recovered to the amount of input catalyst. The degree of increase in yield showed similar shapes when content was low (0.04 mol), but the difference in yield started to increase at 0.06 mol of Mo. Specifically, the yield was about 70 % with 0.03 mol Mo, (200 and 150) % with 0.04 molar Mo. The yields at 0.06 mol Mo were about (680 and 460) %, respectively, which is about 200 % difference. The yields with 0.10 mol of Mo were (1900 and 900) %. The yield with 0.01 mol of Fe was about twice that with 0.02 mol of Fe. As the Mo content increased, the diameters and yields of CNT increased and the crystallinity decreased. These results suggest that Mo accelerates the growth rate of CNT to a larger diameter and at the same time increases the generation of defects in the CNT walls, resulting in higher synthesis yield but lower crystallinity of the CNT. Tang *et al*. [18] studied the optimum conditions for SWNTs by changing the composition of Mo and Co in the Mo-Co/MgO catalyst system. The yield was 11 % when Co was fixed at 0.05 moles. As the content of Mo increased from (0.01 to 0.10) mol, the yield of CNT increased from (40 to 270) %. The almost invisible MWNTs at 0.01 mol accounted for the majority of above 0.75 mol Mo. According to other researchers [19,20], in the case of a catalyst in which the amount of Mo is 5–10 times that of Fe or Co in the Fe-Mo/MgO and Co-Mo/MgO catalysts, the diameter of CNTs was 10–30 nm, and the CNT yield was about 2000 %. CNTs with larger diameters were thought to have been synthesized using a catalyst with a Mo/Fe ratio higher than a specific value. The ratio of Mo/Fe was estimated to be '5' or less in this study. That is, in this

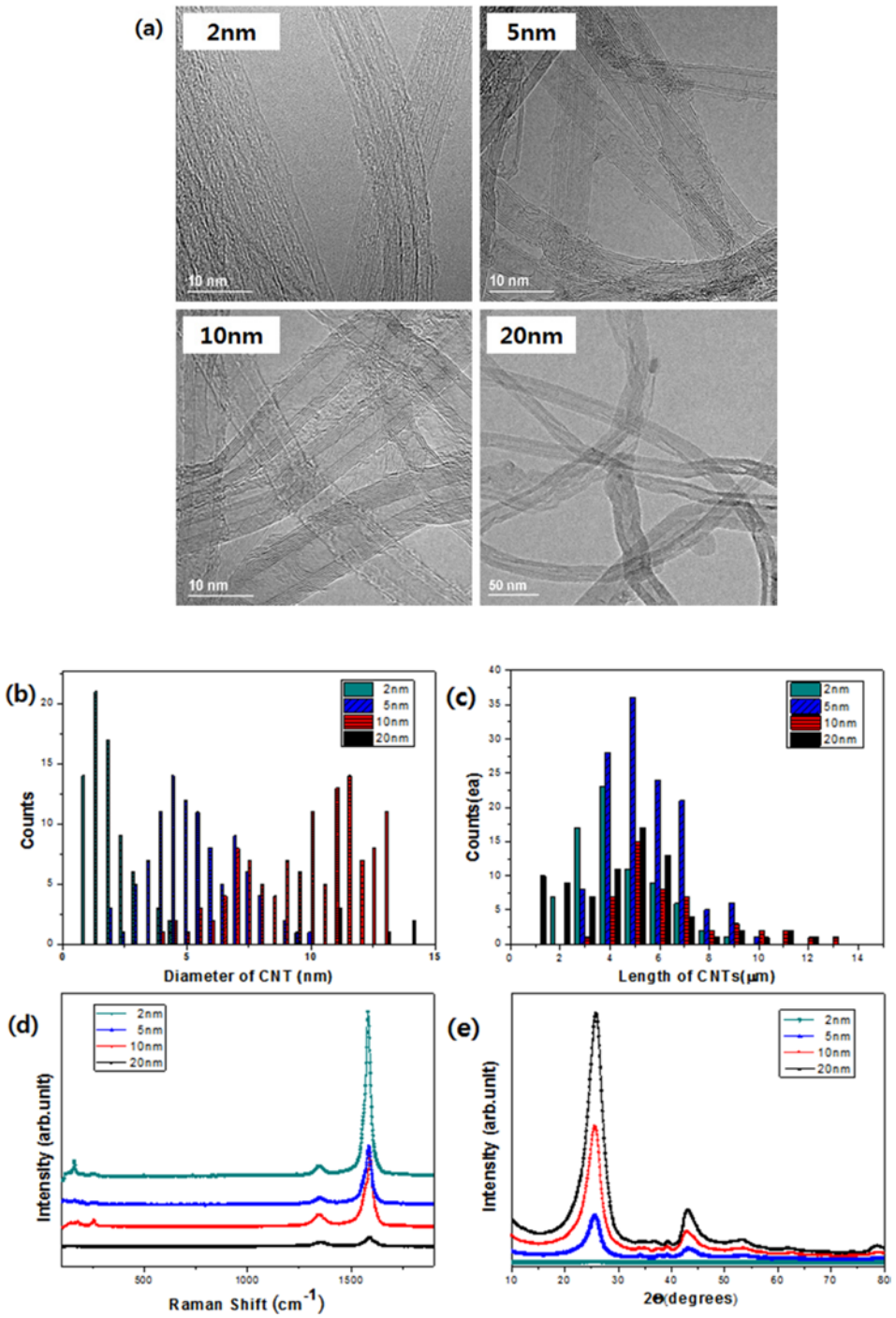

Fig. 2. (a) TEM images, (b) Diameter distributions, (c) Length distributions, (d) Raman spectra, and (e) XRD patterns of four selected CNTs.

paper, CNTs with an average diameter of less than 10 nm and a more uniform diameter distribution were obtained with < 0.05 mol Mo for0.01 mol Fe, and < 0.10 mol Mo for 0.02 mol Fe.

Four CNTs with different diameters but uniform distribution were chosen to determine the effect of diameter on the properties of composite materials. Fig. 2 shows the (a) TEM, (b) diameter distribution, (c) length distribution, (d) Raman spectra, and (e) XRD for the four selected CNTs. Fig. 2(b) shows the diameter distribution of the four CNTs, as measured in the TEM images. It can be seen that each of the four CNTs had a diameter distribution of (1–3, 3–7, 7–13, and 10–30) nm, respectively. To distinguish these CNTs, they were named 2 nm, 5 nm, 10 nm, and 20 nm CNTs, respectively. TEM images in Fig. 2(a), shows that dozens of 2 nm CNTs were aggregated and that the 5 nm CNTs

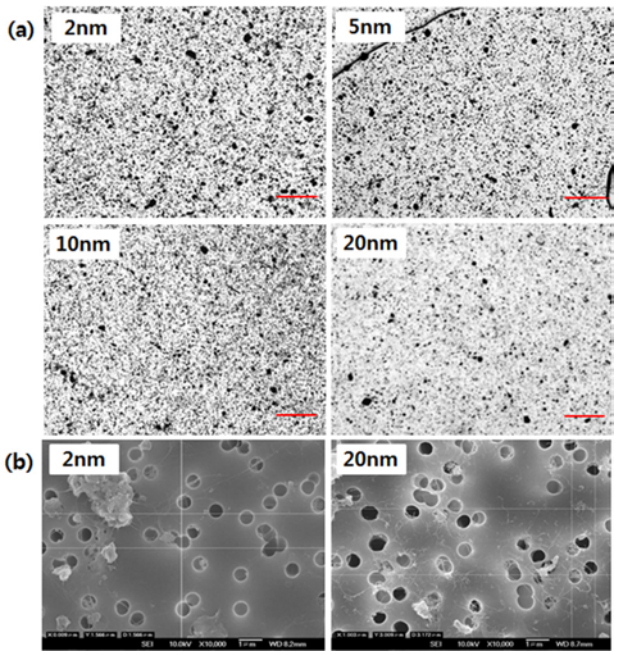

Fig. 3. (a) Optical microscope images of four CNTs in composites and (b) SEM images after homogenizer-milling

consisted of several types of aggregations. The (10 and 20) nm CNTs, having large diameter, have almost no aggregated CNTs. The length distributions of CNTs extracted from dozens of SEM images are shown in Fig. 2(b). As a result of the length measurements, it was determined that the average length was about 4.3 μm for 2 nm CNT, 5.6 μm for 5 nm CNT, 6.4 μm for 10 nm CNT, and 4.9 μm for 20 nm CNT. Moreover, the maximum frequency length for almost all CNTs was about 4–6 μm. For 20 nm CNTs with relatively low crystallinity, the number of CNTs with length of 1 μm or less was very large. The crystallinity of the CNTs was calculated by comparing A_D and A_G from the Raman spectra in Fig. 2(c). The crystallinity of 2 nm CNTs was 0.05, which was almost ten times greater than that of 20 nm CNTs. The value of A_D/A_G for 5 nm CNTs was almost 0.11 and that for 10 nm CNTs was 0.19. Fig. 2(d) shows the XRD patterns of the CNTs used, which show almost the same diffraction C(002) peak at 2θ of 25.6–26.1° corresponding to a d-spacing between graphene sheets of 3.43–3.45 Å. As the CNT diameter increased, the inter-wall distance C (002) decreased. The FWHMs of the C (002) peak were 3.5, 3.3, and 3.2 for (5, 10, and 20) nm CNTs, respectively. The C (100) peak was found around 43.2° due to the lateral correlation of the graphite layer. From the nitrogen adsorption isotherms (not shown here), the specific surface area (SSA) of each CNT was obtained. The SSA of the four sizes of CNTs was (595, 496, 374 and 265) m^2/g according to increasing order of CNT diameter. The reason why the difference in specific surface area between (2 and 5) nm CNT is not very large is related to the formation of CNT aggregations.

Fig. 3 is a micrograph showing a 200-fold magnification of a composite material having CNT content of 0.1 wt%. It was used to examine the dispersion state of each CNT in the composites. From Fig. 3(a), it can be seen that (2 and 5) nm CNTs have a large number of agglomerates. Compared with

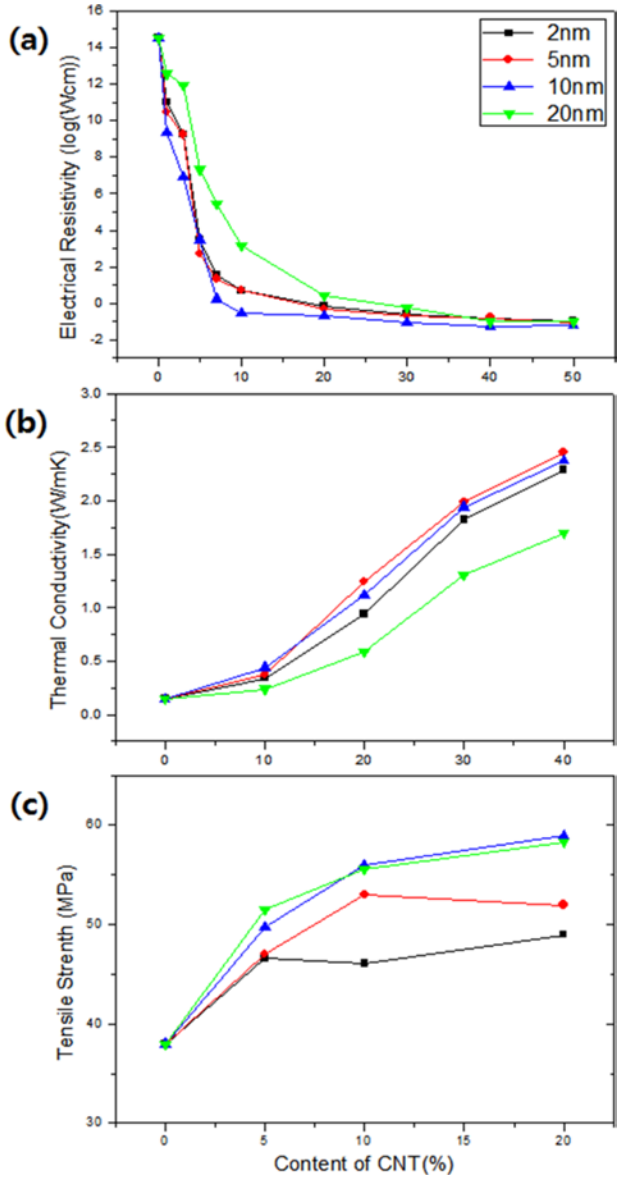

Fig. 4. Properties of CNT-polyamide composites prepared according to CNT diameter and content: (a) Electrical resistance, (b) Thermal conductivity, and (c) Tensile strength.

(10 and 20) nm CNTs, the agglomeration was relatively decreased. Fig. 3(b) is a SEM image used for length analysis. It can be seen that the 2 nm CNTs still have a relatively large number of aggregations after milling, while the 20 nm CNTs are much smaller.

Fig. 4 shows the properties of CNT-polyamide composites including such as (a) electrical resistance, (b) thermal conductivity, and (c) tensile strength according to the CNT diameter and content. As shown in Fig. 4(a), as the content of CNTs as a conductive filler increases, the resistance of each composite decreases sharply regardless of the diameter of CNTs; at saturation the resistance was around 1 Ω. Generally, as the content of conductive filler increased, the composite, which was an insulator, gradually turned into a conductor. This was due to the formation of a

continuous path or conductive network through which electrons could travel through the conductive filler. When the conductive network was formed, that is, when the electrical resistance value of the composite material was generally about 10^6 Ω, the content of the conductive filler was regarded as a percolation threshold value [21]. From Fig. 4a, CNT-polyamide composites with a diameter of 10 nm or less have a threshold value of 5 phr or less, although there was a slight difference depending on the diameter when estimating the threshold value of CNTs having different diameters. On the other hand, the relatively large 20 nm CNTs showed a threshold value between (7 and 10) phr. Threshold values of CNT were different according to CNT used and mixing method, but when CNT was dispersed in epoxy, it showed a low threshold of 0.01–0.10 % [22]. In the cases of polyethylene, polypropylene, and polycarbonate composites, threshold values were about 1–3 % [23]. In contrast, the threshold value of polyamide was relatively high, about 4–7 % [24,25]. Ha *et al*. [26] reported that the polyamide composites had high threshold values because they were involved in the hydrogen bonding of repeated methylene groups in the polyamides. The hydrogen bond inhibited the dispersion of CNT in the polyamide polymer, and the resistance of the composite was not easily lowered even if CNT was added above the critical value. The 10 nm CNT composite had a resistance value of less than 100 Ω at 7 phr and the electric conductivity was almost saturated at 10 phr. On the other hand, the resistance of composites with (2 and 5) nm CNTs was nearly 100 Ω at 10 phr and was saturated at 20 phr. However, the 20 nm CNT composites exhibited a resistance value of about 100 Ω at 20 phr and a saturation value of 1 Ω at 40 phr. The (2 and 5) nm CNTs were expected to show lower resistance values among the composites because of the relatively large number of CNTs with the same content. However, 10 nm CNTs were suitable for composites. This is due to the formation of aggregations of (2 and 5) nm CNTs, as shown in Fig. 2. Hou *et al*. [14] reported that SWNTs have good crystallinity, but SWNT composites exhibit low electrical conductivity due to low dispersion and formation of aggregations. In addition, if the diameter is larger, the electrical conductivity of the composite is reduced due to its low crystallinity and low aspect ratio (length to diameter ratio) despite its relatively high dispersion.

The vertical thermal conductivity of the CNT-polyamide composite is shown in Fig. 3(b). As the CNT content increases, the thermal conductivity of the composite gradually increases. The thermal conductivity of composites using small diameter CNTs such as 2–10 nm CNT, reached almost 2.4 W/m·K at 40 phr and this was about 1500 % higher than the thermal conductivity of neat polyamide. In contrast, the 20 nm CNT composite had a thermal conductivity of 1.7 W/m·K at 40 phr CNT, about an 1100 % increase. However, the increase was smaller than expected. The thermal conductivity increase rate of (2, 5, and 10) nm CNT was (0.53–0.56, 0.57–0.61, and 0.56–0.60) W/m·K, respectively. On the other hand, the rate of increase in thermal conductivity for 20 nm CNT was 0.38 W/m·K. The Lewis-Liesen model was used to predict the thermal conductivity according to the CNT diameter and content. As a result, the composite thermal conductivity according to diameter was estimated to be from (1.5 to 2.0) W/m·K at 10 phr and from (4.0 to 6.0) W/m·K at 40 phr. The explanation for the difference between the calculated value and the experimental value can be deduced from a review paper [27]. The thermal interface resistance phenomenon was the biggest of the bottlenecks in the manufacture of CNT-polymer composites with excellent thermal conductivity. There was high thermal resistance between CNT and the matrix polymer. There was also thermal resistance between CNTs due to low thermal contact efficiency and contact area. For this reason, the thermal contact area of 2 nm CNTs was smaller than of 10 nm CNTs, and the heat resistance was relatively higher. Therefore, 2nm CNT composites showed lower thermal conductivity than 10 nm CNT composites did. In addition, 20 nm CNTs are shorter than 10 nm CNTs, resulting in relatively poor thermal contact efficiency. This degraded the thermal conductivity of the composite material.

Fig. 3(c) shows the tensile strength of CNT-polyamide composites according to the CNT diameter and content. The elongation of the composite material was 5 mm/min. Tensile tests could not be carried out because the composites with CNT content of 30 phr or more is too fragile. The tensile strength of neat polyamide was measured up to 37 MPa and the tensile strength of CNT-added composites increased to 60 MPa according to CNT diameter. The strength of smaller diameter CNTs such as (2 and 5) nm CNTs, decreased with increasing CNT content. Composites of (10 and 20) nm CNTs with large diameters showed a continuous increase in strength up to 20 phr. As described above, because CNTs in the composite material are relatively large, the tensile properties of the small-diameter CNTs were not improved and they easily agglomerated. The 20 nm CNTs was easily cut in the homogenizer and during sonification due to their low crystallinity, the result of many defects.

To control the CNT diameter, CVD synthesis for CNTs with different diameter distributions was carried out by increasing Mo. As Mo was enriched in Mo-Fe/MgO catalysts, both the diameter and yield of CNTs increased, but the crystallinity decreased. However, if the Mo content was increased above a specific ratio to Fe, the synthesized CNT would have a higher yield, wider diameter distribution, and lower crystallinity. To investigate the relationship between CNT diameters and the properties of the composites, four CNTs with different diameter distributions were selected to produce polyamide composites. The properties of the composites were evaluated using electrical resistance, thermal conductivity, and tensile strength. The characteristics of the composites prepared with CNTs with an average diameter of 10 nm or less, were superior to those composites in which CNT had an average diameter of 20 nm. Among the CNTs with a diameter of 10 nm or less, CNTs having an average diameter of 10 nm was considered to be most suitable for use in composite material. It showed a threshold of electrical resistance of 5 phr or less, a thermal conductivity of 2.4 W/m·K at 40 phr, and a tensile strength of 60 MPa at 20 phr.

Acknowledgements

This work was supported by research grants provided by Industrial Technology Innovation Program(No.10052724) under the Ministry of Trade, Industry & Energy and the Defense Acquisition Program Administration (No. 15-CM-MA-15).

References

[1] Ebbesen TW, Lezec HJ, Hiura H, Bennett JW, Ghaemi HF, Thio T. Electrical conductivity of individual carbon nanotubes. Nature, 382, 54 (1996) DOI:10.1038/382054a0

[2] Jianwei C, Tahir C, William AG. Thermal conductivity of carbon nanotubes. Nanotechnology, 11, 65 (2000) DOI:10.1088/0957-4484/11/2/305

[3] Salvetat JP, Bonard JM, Thomson NH, Kulik AJ, Forro L, Benoit W, Zuppiroli L. Mechanical properties of carbon nanotubes. App Phy A, 69, 255 (1999) DOI:10.1007/s003390050999

[4] Fujii M, Zhang X, Xie H, Ago H, Takahashi K. Measuring the thermal conductivity of a single carbon nanotube. Phys Rev Lett, 6, 065502 (2005) DOI: 10.1103/PhysRevLett.95.065502

[5] Ruoff RS, Qian D, Liu KM. Mechanical properties of carbon nanotubes: theoretical predictions and experimental measurements. C R Physique, 4, 993 (2003) DOI: 10.1016/j.crhy.2003.08.001

[6] Zeng Y, Liu P, Du JH, Zhao L, Ajayan PM, Cheng HM. Increasing the electrical conductivity of carbon nanotube/polymer composites by using weak nanotube–polymer interactions. Carbon, 48, 3551 (2010) DOI:10.1016/j.carbon.2010.05.053

[7] Hou C, Li T, Zhao T, Whang W, Cheng Y. Electromagnetic wave absorbing properties of carbon nanotubes doped rare metal/pure carbon nanotubes double-layer polymer composites. Materials & Design, 33, 413 (2012) DOI: 10.1016/j.matdes.2011.04.042

[8] Wang X, Yong ZZ, Lib QW, Bradford PD, Liu W, Tucker DS, Ca W, Wang H, Yuan FG, Zhu YT. Ultrastrong, stiff and multifunctional carbon nanotube composites, Mater Res Lett, 1, 19 (2013) DOI:10.1080/21663831.2012.686586

[9] Wu ML, Chen Y, Zhang L, Zhan H, Qiang L, Wang.NJ. High-performance carbon nanotube/polymer composite fiber from layer-by-layer deposition. Appl Mater Interfaces, 8, 8137 (2016) DOI: 10.1021/acsami.6b01130

[10] Collins PG. Defects and disorder in carbon nanotubes. Oxford Handbook of Nanoscience and Technology: Volume 2: Materials: Structures, Properties and Characterization Techniques, 2, 31 (2010).

[11] Kis A, Zettl A. Nanomechanics of carbon nanotubes. Phil Trans R Soc A, 366, 1591 (2008) DOI:10.1098/rsta.2007.2174

[12] Cheung CL, Kurtz A, Park HK, Lieber CM. Diameter-controlled synthesis of carbon nanotubes, J Phys Chem B, 106, 2429 (2002) DOI: 10.1021/jp0142278

[13] Ding F, Rosén A, Bolton K. Molecular dynamics study of the catalyst particle size dependence on carbon nanotube growth. J Chem Phys 8, 2775 (2004) DOI: 10.1063/1.1770424

[14] Hou Y, Tang J, Zhang H, Qian C, Feng Y, Liu J. Functionalized few-walled carbon nanotubes for mechanical reinforcement of polymeric composites. ACS Nano, 3, 1057 (2009) DOI: 10.1021/nn9000512

[15] Labunov VA, Basaev AS, Shulitski BG, Shaman YP, Komissarov I, Prudnikava AL, Tay BK, Shakerzadeh M. Growth of few-wall carbon nanotubes with narrow diameter distribution over Fe-Mo-MgO catalyst by methane/acetylene catalytic decomposition. Nanoscale Res Lett 7, 102 (2012) DOI: 10.1186/1556-276X-7-102

[16] Martín O, Gutierrez HR, Valiente AM, Terrones M, Blanco T, Baselga J. An efficient method for the carboxylation of few-wall carbon nanotubes with little damage to their sidewalls. Mater Chem Phys, 140, 499 (2013) DOI: 10.1016/S0009-2614(01)01183-6

[17] Park YS, Moon HS, Huh MY, Kim BJ, Kuk YS, Kang SJ, Lee SH, An KY. Synthesis of aligned and length-controlled carbon nanotubes by chemical vapor deposition. Carbon letters, 14, 99 (2013) DOI: 10.5714/CL.2013.14.2.099

[18] Tang S, Zhong Z, Xiong Z, Sun L, Liu L, Lin j, Shen ZX, Tan KL. Controlled growth of single-walled carbon nanotubes by catalytic decomposition of CH4 over Mo/Co/MgO catalysts. Chem Phys Lett 300 19 (2001) DOI:10.1016/S0009-2614(01)01183-6

[19] Santhosh C, Saranya M, Felix S, Ramachandran R, Pradeep N, Uma V, Grace AN. Growth of carbon nanotubes using MgO supported Mo-Co catalysts by thermal chemical vapor deposition technique. J Nano Res. 24, 46 (2013) DOI: 10.4028/www.scientific.net/JNanoR.24.46

[20] Pérez MM, Vallés C, Maser WK, Martínez MT, Benito AM. Influence of molybdenum on the chemical vapour deposition production of carbon nanotubes. Nanotechnology, 16, S224 (2005) DOI: 10.1088/0957-4484/16/5/016.

[21] Garboczi EJ, Snyder KA, Douglas JF, Thorpe MF. Geometrical percolation threshold of overlapping ellipsoids. Phys Rev E Stat Phys Plasmas Fluids Relat Interdiscip Topics, 52, 819 (1995) DOI: 10.1103/PhysRevE.52.819

[22] Kausar A, Rafique I, Muhammad B. Review of applications of polymer/carbon nanotubes and epoxy/CNT composites. J Polym Plas Tech Eng, 55, 1167 (2016) DOI: 10.1080/03602559.2016.1163588

[23] Dul JH, Bai J, Cheng HM. The present status and key problems of carbon nanotube based polymer composites. J eXPRESS Polym Lett 1, 253 (2007) DOI: 10.3144/expresspolymLett.2007.39

[24] Ryu J, Han MJ, Improvement of the mechanical and electrical properties of polyamide 6 nanocomposites by non-covalent functionalization of multi-walled carbon nanotubes. Comp Sci Tech, 102, 169 (2014) DOI: 10.1016/j.compscitech.2014.07.022

[25] Bauhofer W, Kovacs JZ, A review and analysis of electrical percolation in carbon nanotube polymer composites. Comp Sci Tech. 69, 1486 (2009) DOI: 10.1016/j.compscitech.2008.06.018

[26] Ha HJ, Kim SC, Ha, KR. Morphology and properties of polyamide/multi-walled carbon nanotube composites. Macromolecular Research, 18, 660 (2010) DOI: 10.1007/s13233-010-0702-y

[27] Han Z, Fina A. Thermal conductivity of carbon nanotubes and their polymer nanocomposites: A review, Progress in Polymer Science, 36, 914–944 (2010) DOI: 10.1016/j.progpolymsci.2010.11.004